Acta Mechanica Solida Sinica, Vol. 27, No. 5, October, 2014 ISSN 0894-9166
Published by AMSS Press, Wuhan, China

NONLINEAR TRANSIENT RESPONSE OF FUNCTIONALLY GRADED SHALLOW SPHERICAL SHELLS SUBJECTED TO MECHANICAL LOAD AND UNSTEADY TEMPERATURE FIELD**

Yiming Fu **Sumin Hu*** **Yiqi Mao**

(*College of Mechanical and Vehicle Engineering, Hunan University, Changsha* 410082*, China*)

Received 20 November 2012, revision received 5 March 2014

ABSTRACT This paper is concerned with the transient deformation of functionally graded (FG) shallow spherical shells subjected to time-dependent thermomechanical load. Based on Timoshenko-Mindlin hypothesis and von Karman nonlinear theory, a set of nonlinear governing equations of motion for FG shallow spherical shells in regard to transverse shear deformation and all the inertia terms are established using Hamilton's principle. The collocation point method and Newmark-beta scheme in conjunction with the finite difference method are adopted to solve the governing equations of motion and the unsteady heat conduction equation numerically. In the numerical examples, the transient deflection and stresses of FG shallow spherical shells with various material properties under different loading conditions are presented.

KEY WORDS functionally graded materials, unsteady temperature field, transient deflection and stresses

I. INTRODUCTION

The concept of functionally graded materials (FGMs) was first introduced in 1984 by materials scientists in the Sendai area of Japan[1]. FGMs refer to heterogeneous composite materials. The composition of FGMs varies continuously from one surface of the materials to the other, resulting in continuously varying material properties. FGMs are usually made from a mixture of metal and ceramic that combines the advantages of toughness, machinability of metal and high strength, temperature resistance of ceramic. Therefore, FGMs have found potential applications in aerospace, biomedical, and energy engineering. And FGMs structures are not merely under mechanical load, but also frequently in a temperature field.

In recent years, a lot of research have been performed on the analysis of FG structures subjected to mechanical load in a steady temperature field. Shen[2] employed a mixed Galerkin-perturbation technique to study the bending response of FG plates in thermal environment. Pelletier et al.[3] obtained an exact solution for the thermoelastic response of FG orthotropic cylindrical shells. A FG anisotropic cylinder in different thermomechanical states was studied via Fourier series by Tarn[4]. Woo et al.[5] presented an analytical solution for the postbuckling of FG moderately thick plates and shallow shells under the condition of compressive loads and steady temperature fields. The thermomechanical postbuckling of a FG circular plate was investigated by Ma et al.[6]. Using the higher-order shear deformation theory,

* Corresponding author. E-mail: hu_sumin@hnu.edu.cn

** Project supported by the National Natural Science Foundation of China (No. 11072076).

Alijani et al.[7] employed the pseudo-arclength continuation and collocation scheme to study the thermal effects on the vibrations of FG doubly curved shells. Shahsiah et al.[8] studied thermal instability of FG shallow spherical shells, and the critical buckling temperatures were discussed for three types of thermal loads, respectively. Praveen and Reddy[9] investigated the nonlinear thermoelastic response of FG plates using the finite element method (FEM).

The transient behaviours of FGMs in unsteady temperature fields have not drawn much attention. Wang et al.[10] investigated the thermal shock behaviours of FG plates. Using the AEH and finite element methods, Goupee et al.[11] studied the transient thermoelastic response of FGMs. Kim and Noda[12] investigated the deflection and transient temperature distribution of FG plates using a Green's function approach. Introducing a laminated plate model, Tanigawa et al.[13] analyzed the thermal stresses of FG plates. Jin and Paulino[14] studied an edge crack in a strip of FGM under transient thermal load conditions. Asgari and Akhlaghi[15] investigated the temperature, displacements and stresses of a FG thick hollow cylinder of finite length using the FEM. Vel and Batra[16] presented an analytical solution for analyzing the transient temperature, displacements and thermal stresses of FG plates subjected to time-dependent thermal loads. Qian and Batra[17] obtained the transient temperature distribution in a thick FG plate using meshless local Petrov-Galerkin method (MLPG). Mahmoud et al.[18] studied the elasto-plastic behaviours of FGMs under thermal loads by adopting a stress-strain power law hardening model.

To the best of the authors' knowledge, open literature in this field were limited to the analysis of FG structures in either a steady temperature field or unsteady temperature field without mechanical load. To date, no research is reported on the transient behaviours of FG shallow spherical shells subjected to mechanical loads in an unsteady temperature field. In the present paper, a model for a FG shallow spherical shell subjected to time-dependent thermomechanical loads is presented. The transient temperature is determined from the heat conduction equation using the finite difference method. The displacement functions are divided between space and time domains with the collocation point method and Newmark-beta method, respectively. By combining the governing equations of motion, boundary conditions and initial conditions, the whole problem is solved with the iterative method.

II. BASIC EQUATIONS

Consider a FG shallow spherical shell shown in Fig.1, in which R, h, a are the curvature radius of the middle curved surface, the thickness of the shell and the radius of the base circle, respectively. An arbitrary point in the shell can be determined by the orthogonal curvilinear coordinates (φ, θ) on the middle curved surface and z coordinate along the inner normal direction of the middle curved surface. The complementary angle of latitude φ is measured from the axisymmetric axis, and the longitude θ is measured from any radius of a parallel circle. $z = 0$ denotes the middle curved surface, and $z = \pm h/2$ denotes inner and outer surfaces of the shell, respectively. In the given orthogonal curvilinear coordinates, the principal radii of curvature are $R_1 = R_2 = R$, the Lamé coefficients of the middle curved surface are $A = R$ and $B = R\sin\varphi$ and the principal curvatures are $\kappa_1 = \kappa_2 = -1/R$.

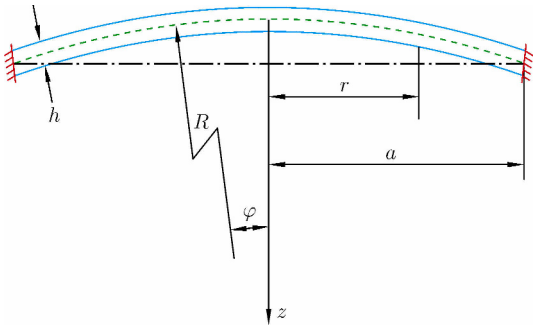

Fig. 1. Geometrical configuration of FG shallow spherical shell.

2.1. Geometric Relations

In the case of the axisymmetric deformations of a FG shallow spherical shell, the circumferential displacement $u_2 = 0$, and all the variables are independent of θ. Based on the Timoshenko-Mindlin hypothesis, the displacement components (u_1, u_2, u_3) of an arbitrary point in the shallow spherical shell along the coordinate (φ, θ, z) at any time t are expressed as

$$\begin{aligned} u_1(r,\theta,z,t) &= u(r,t) + z\phi(r,t) \\ u_2(r,\theta,z,t) &= 0 \\ u_3(r,\theta,z,t) &= w(r,t) \end{aligned} \tag{1}$$

where (u, w) are the displacement components of the corresponding point on the middle curved surface along the (φ, z) directions, respectively. ϕ is the rotation angles of the normal to middle surface along the φ direction.

According to von Karman nonlinear theory, the strain components (ε_φ, ε_θ, $\varepsilon_{\varphi z}$) of an arbitrary point in the shallow spherical shell can be expressed as

$$\varepsilon_\varphi = \varepsilon_{\varphi,0} + z\kappa_\varphi, \quad \varepsilon_\theta = \varepsilon_{\theta,0} + z\kappa_\theta, \quad \varepsilon_{\varphi z} = \phi + \frac{\partial w}{R\partial\varphi} \tag{2}$$

in which $\varepsilon_{\varphi,0}$, $\varepsilon_{\theta,0}$ are the strain components on the middle curved surface and κ_φ, κ_θ are the changed values of the curvatures on the middle curved surface, and

$$\varepsilon_{\varphi,0} = \frac{\partial u}{R\partial\varphi} - \frac{w}{R} + \frac{1}{2}\left(\frac{\partial w}{R\partial\varphi}\right)^2, \quad \varepsilon_{\theta,0} = \frac{u}{R}\cot\varphi - \frac{w}{R}, \quad \kappa_\varphi = \frac{\partial\phi}{R\partial\varphi}, \quad \kappa_\theta = \frac{\phi}{R}\cot\varphi \tag{3}$$

In the analysis of the shallow spherical shell, introducing a new coordinate r along the direction of the radius of the base circle, using the following approximate relations $r \approx R\varphi$, $\sin\varphi \approx \varphi$, $\cos\varphi \approx 1$, and substituting those approximate relations into Eqs.(2) and (3), we have

$$\varepsilon_{\varphi,0} = \frac{\partial u}{\partial r} - \frac{w}{R} + \frac{1}{2}\left(\frac{\partial w}{\partial r}\right)^2, \quad \varepsilon_{\theta,0} = \frac{u}{r} - \frac{w}{R}, \quad \kappa_\varphi = \frac{\partial\phi}{\partial r}, \quad \kappa_\theta = \frac{\phi}{r}, \quad \varepsilon_{\varphi z} = \phi + \frac{\partial w}{\partial r} \tag{4}$$

2.2. Constitutive Relations

Consider the influence of a one-dimensional unsteady state temperature field on the transient behaviours of a FG shallow spherical shell. The temperature of the shell on the top surface ($z = -h/2$) is assumed to be different from that on the bottom surface ($z = h/2$), but constant in-plane. The temperature distribution along the thickness direction can be determined from the following one-dimensional unsteady state heat transfer equation[19]:

$$\frac{\partial}{\partial z}\left[k(z)\frac{\partial T(z,t)}{\partial z}\right] - \rho(z)c(z)\frac{\partial T(z,t)}{\partial t} = 0 \tag{5}$$

in which $k(z)$, $\rho(z)$ and $c(z)$ are thermal conductivity , mass density and specific heat of the shallow spherical shell, respectively. The temperature on the top and that on the bottom surfaces of the shell are T_t and T_b, respectively. The stress free temperature is assumed to be zero. Then the temperature increment $\Delta T(z, t)$ of any point in the shell is equal to $T(z, t)$.

For FG shallow spherical shells, the material properties, such as elastic stiffness $E(z)$, thermal conductivity $k(z)$, coefficient of thermal expansion $\alpha(z)$, specific heat $c(z)$ and mass density $\rho(z)$ vary through the thickness of the shell as a simple power function[20] as follows:

$$P(z) = P_c + (P_m - P_c)\left(\frac{2z+h}{2h}\right)^n \tag{6}$$

where n is the volume fraction index, and P_m and P_c are corresponding properties of the metal and ceramic, respectively.

Therefore, with the temperature effect and the material properties varying along the thickness direction as a simple power function, the thermoelastic constitutive relations of FG shallow spherical shell can be expressed as

$$\left\{\begin{array}{c}\sigma_\varphi\\ \sigma_\theta\\ \sigma_{\varphi z}\end{array}\right\}=\left[\begin{array}{ccc}C_{11} & C_{12} & 0\\ C_{21} & C_{22} & 0\\ 0 & 0 & C_{44}\end{array}\right]\left(\left\{\begin{array}{c}\varepsilon_\varphi\\ \varepsilon_\theta\\ \varepsilon_{\varphi z}\end{array}\right\}-\left\{\begin{array}{c}\alpha(z)\\ \alpha(z)\\ 0\end{array}\right\}T(z,t)\right) \tag{7}$$

in which σ_φ, σ_θ, $\sigma_{\varphi z}$ are the stress components of any point in the shell, and

$$C_{11}=C_{22}=\frac{E(z)}{1-\nu^2},\quad C_{12}=C_{21}=\nu C_{11},\quad C_{44}=\frac{E(z)}{2\,(1+\nu)}$$

2.3. Nonlinear Governing Equations of Motion

The Lamé coefficients of any point in the shallow spherical shell are $H_1=A_1(1-z/R_1)$, $H_2=A_2(1-z/R_2)$. And there exists the following appropriate relations $1-z/R_1\approx 1$, $1-z/R_2\approx 1$ for the shallow spherical shell. By taking all the inertia terms into account, the nonlinear governing equations of motion for FG shallow spherical shell under thermomechanical loads can be derived from the Hamilton's principle as[21]

$$\frac{\partial rN_\varphi}{r\partial r}-\frac{N_\theta}{r}=I_0\frac{\partial^2 u}{\partial t^2}+I_1\frac{\partial^2\phi}{\partial t^2} \tag{8}$$

$$\frac{1}{R}(N_\varphi+N_\theta)+\frac{\partial}{r\partial r}\left(rN_\varphi\frac{\partial w}{\partial r}\right)+\frac{\partial}{r\partial r}(rQ_{\varphi z})+q=I_0\frac{\partial^2 w}{\partial t^2} \tag{9}$$

$$\frac{\partial rM_\varphi}{r\partial r}-\frac{M_\theta}{r}-Q_{\varphi z}=I_0\frac{\partial^2 u}{\partial t^2}+I_2\frac{\partial^2\phi}{\partial t^2} \tag{10}$$

where $(N_\varphi,\,N_\theta)$ and $(M_\varphi,\,M_\theta)$ are the membrane stress resultants and membrane stress couples, respectively, and $Q_{\varphi z}$ are the transverse shear stress resultant, which are calculated from the following integral expressions:

$$(N_\varphi,M_\varphi)=\int_{-h/2}^{h/2}\sigma_\varphi\,(1,z)\mathrm{d}z,\quad (N_\theta,M_\theta)=\int_{-h/2}^{h/2}\sigma_\theta\,(1,z)\mathrm{d}z,\quad Q_{\varphi z}=K\int_{-h/2}^{h/2}\sigma_{\varphi z}\mathrm{d}z \tag{11}$$

where K is the shear correction factor and the inertia coefficients $I_i\,(i=0,\,1,\,2)$ are defined as

$$(I_0,I_1,I_2)=\int_{-h/2}^{h/2}\rho\,(z)\left(1,z,z^2\right)\mathrm{d}z$$

Then from Eqs.(2), (7) and (11), one can get

$$\begin{aligned}
N_\varphi&=A_{11}\varepsilon_{\varphi,0}+B_{11}\kappa_\varphi+A_{12}\varepsilon_{\theta,0}+B_{12}\kappa_\theta-\int_{-h/2}^{h/2}(C_{11}+C_{12})\,\alpha T\mathrm{d}z\\
N_\theta&=A_{21}\varepsilon_{\varphi,0}+B_{21}\kappa_\varphi+A_{22}\varepsilon_{\theta,0}+B_{22}\kappa_\theta-\int_{-h/2}^{h/2}(C_{21}+C_{22})\,\alpha T\mathrm{d}z\\
M_\varphi&=B_{11}\varepsilon_{\varphi,0}+D_{11}\kappa_\varphi+B_{12}\varepsilon_{\theta,0}+D_{12}\kappa_\theta-\int_{-h/2}^{h/2}z\,(C_{11}+C_{12})\,\alpha T\mathrm{d}z\\
M_\theta&=B_{21}\varepsilon_{\varphi,0}+D_{21}\kappa_\varphi+B_{22}\varepsilon_{\theta,0}+D_{22}\kappa_\theta-\int_{-h/2}^{h/2}z\,(C_{21}+C_{22})\,\alpha T\mathrm{d}z\\
Q_{\varphi z}&=G\varepsilon_{\varphi z}
\end{aligned} \tag{12}$$

where A_{ij}, B_{ij}, D_{ij} and G are the shell stiffness coefficients, which are given by

$$(A_{ij},B_{ij},D_{ij})=\int_{-h/2}^{h/2}C_{ij}(1,z,z^2)\mathrm{d}z\;\;(i,j=1,2)\,,\quad G=\int_{-h/2}^{h/2}C_{44}\mathrm{d}z \tag{13}$$

Introduce the following dimensionless parameters:

$$\bar{r}=\frac{r}{a},\quad \bar{u}=\frac{a}{h^2}u,\quad \bar{\phi}=\frac{a}{h}\phi,\quad \bar{w}=\frac{w}{h},\quad \lambda_1=\frac{h}{a},\quad \lambda_2=\frac{a}{R},\quad \bar{z}=\frac{z}{h},\quad \bar{A}_{ij}=\frac{A_{ij}}{E_m h}$$
$$\bar{B}_{ij}=\frac{B_{ij}}{E_m h^2},\quad \bar{D}_{ij}=\frac{D_{ij}}{E_m h^3},\quad \bar{G}=\frac{G}{E_m h},\quad \bar{I}_0=\frac{I_0}{\rho_m h},\quad \bar{I}_1=\frac{I_1}{\rho_m h^2},\quad \bar{I}_2=\frac{I_2}{\rho_m h^3} \tag{14}$$
$$\bar{q}=\frac{q}{E_m\lambda_1^4},\quad \tau=t\sqrt{\frac{E_m}{\rho_m a^2}},\quad \bar{C}_{11}=\frac{C_{11}}{E_m},\quad \bar{C}_{12}=\frac{C_{12}}{E_m},\quad \bar{C}_{21}=\frac{C_{21}}{E_m},\quad \bar{C}_{22}=\frac{C_{22}}{E_m}$$

By substituting Eq.(12) into Eqs.(8), (9) and (10), and using the Eqs.(4) and (14), the dimensionless nonlinear governing equations of motion for FG shallow spherical shell can be expressed as

$$\begin{aligned}&\left(\bar{A}_{11}-\bar{A}_{21}\right)\left[\frac{\partial\bar{u}}{\partial\bar{r}}-\frac{\lambda_2}{\lambda_1}\bar{w}+\frac{1}{2}\left(\frac{\partial\bar{w}}{\partial\bar{r}}\right)^2\right]+\left(\bar{B}_{11}-\bar{B}_{21}\right)\frac{\partial\bar{\phi}}{\partial\bar{r}}+\left(\bar{A}_{12}-\bar{A}_{22}\right)\left(\frac{\bar{u}}{\bar{r}}-\frac{\lambda_2}{\lambda_1}\bar{w}\right)+\left(\bar{B}_{12}-\bar{B}_{22}\right)\frac{\bar{\phi}}{\bar{r}}\\&+\bar{r}\left[\bar{A}_{11}\left(\frac{\partial^2\bar{u}}{\partial\bar{r}^2}-\frac{\lambda_2\partial\bar{w}}{\lambda_1\partial\bar{r}}+\frac{\partial\bar{w}}{\partial\bar{r}}\frac{\partial^2\bar{w}}{\partial\bar{r}^2}\right)+\bar{B}_{11}\frac{\partial^2\bar{\phi}}{\partial\bar{r}^2}+\bar{A}_{12}\left(\frac{\partial\bar{u}}{\bar{r}\partial\bar{r}}-\frac{\bar{u}}{\bar{r}^2}-\frac{\lambda_2\partial\bar{w}}{\lambda_1\partial\bar{r}}\right)+\bar{B}_{12}\left(\frac{\partial\bar{\phi}}{\bar{r}\partial\bar{r}}-\frac{\bar{\phi}}{\bar{r}^2}\right)\right]\\&-\frac{1}{\lambda_1^2}\left[\int_{-1/2}^{1/2}\left(\bar{C}_{11}+\bar{C}_{12}\right)\alpha T\mathrm{d}\bar{z}-\int_{-1/2}^{1/2}\left(\bar{C}_{21}+\bar{C}_{22}\right)\alpha T\mathrm{d}\bar{z}\right]=\bar{I}_0\bar{r}\frac{\partial^2\bar{u}}{\partial\tau^2}+\bar{I}_1\bar{r}\frac{\partial^2\bar{\phi}}{\partial\tau^2}\end{aligned} \tag{15}$$

$$\begin{aligned}&\frac{\lambda_2\bar{r}}{\lambda_1}\left\{\left(\bar{A}_{11}+\bar{A}_{21}\right)\left[\frac{\partial\bar{u}}{\partial\bar{r}}-\frac{\lambda_2}{\lambda_1}\bar{w}+\frac{1}{2}\left(\frac{\partial\bar{w}}{\partial\bar{r}}\right)^2\right]+\left(\bar{B}_{11}+\bar{B}_{21}\right)\frac{\partial\bar{\phi}}{\partial\bar{r}}+\left(\bar{A}_{12}+\bar{A}_{22}\right)\left(\frac{\bar{u}}{\bar{r}}-\frac{\lambda_2}{\lambda_1}\bar{w}\right)\right.\\&\left.+\left(\bar{B}_{12}+\bar{B}_{22}\right)\frac{\bar{\phi}}{\bar{r}}-\frac{1}{\lambda_1^2}\left[\int_{-1/2}^{1/2}\left(\bar{C}_{11}+\bar{C}_{12}\right)\alpha T\mathrm{d}\bar{z}+\int_{-1/2}^{1/2}\left(\bar{C}_{21}+\bar{C}_{22}\right)\alpha T\mathrm{d}\bar{z}\right]\right\}\\&+\bar{r}\frac{\partial\bar{w}}{\partial\bar{r}}\left[\bar{A}_{11}\left(\frac{\partial^2\bar{u}}{\partial\bar{r}^2}-\frac{\lambda_2\partial\bar{w}}{\lambda_1\partial\bar{r}}+\frac{\partial\bar{w}}{\partial\bar{r}}\frac{\partial^2\bar{w}}{\partial\bar{r}^2}\right)+\bar{B}_{11}\frac{\partial^2\bar{\phi}}{\partial\bar{r}^2}+\bar{A}_{12}\left(\frac{\partial\bar{u}}{\bar{r}\partial\bar{r}}-\frac{\bar{u}}{\bar{r}^2}-\frac{\lambda_2\partial\bar{w}}{\lambda_1\partial\bar{r}}\right)\right.\\&\left.+\bar{B}_{12}\left(\frac{\partial\bar{\phi}}{\bar{r}\partial\bar{r}}-\frac{\bar{\phi}}{\bar{r}^2}\right)\right]+\left(\bar{r}\frac{\partial^2\bar{w}}{\partial\bar{r}^2}+\frac{\partial\bar{w}}{\partial\bar{r}}\right)\left\{\bar{A}_{11}\left[\frac{\partial\bar{u}}{\partial\bar{r}}-\frac{\lambda_2}{\lambda_1}\bar{w}+\frac{1}{2}\left(\frac{\partial\bar{w}}{\partial\bar{r}}\right)^2\right]+\bar{B}_{11}\frac{\partial\bar{\phi}}{\partial\bar{r}}\right.\\&\left.+\bar{A}_{12}\left(\frac{\bar{u}}{\bar{r}}-\frac{\lambda_2}{\lambda_1}\bar{w}\right)+\bar{B}_{12}\frac{\bar{\phi}}{\bar{r}}-\frac{1}{\lambda_1^2}\int_{-1/2}^{1/2}\left(\bar{C}_{11}+\bar{C}_{12}\right)\alpha T\mathrm{d}\bar{z}\right\}+\frac{1}{\lambda_1^2}\bar{G}\bar{r}\left(\frac{\partial\bar{\phi}}{\partial\bar{r}}+\frac{\partial^2\bar{w}}{\partial\bar{r}^2}\right)\\&+\frac{1}{\lambda_1^2}\bar{G}\left(\bar{\phi}+\frac{\partial\bar{w}}{\partial\bar{r}}\right)+\bar{r}\bar{q}=\frac{\bar{I}_0\bar{r}}{\lambda_1^2}\frac{\partial^2\bar{w}}{\partial\tau}\end{aligned} \tag{16}$$

$$\begin{aligned}&\left(\bar{B}_{11}-\bar{B}_{21}\right)\left[\frac{\partial\bar{u}}{\partial\bar{r}}-\frac{\lambda_2}{\lambda_1}\bar{w}+\frac{1}{2}\left(\frac{\partial\bar{w}}{\partial\bar{r}}\right)^2\right]+\left(\bar{D}_{11}-\bar{D}_{21}\right)\frac{\partial\bar{\phi}}{\partial\bar{r}}+\left(\bar{B}_{12}-\bar{B}_{22}\right)\left(\frac{\bar{u}}{\bar{r}}-\frac{\lambda_2}{\lambda_1}\bar{w}\right)\\&+\left(\bar{D}_{12}-\bar{D}_{22}\right)\frac{\bar{\phi}}{\bar{r}}+\bar{r}\left[\bar{B}_{11}\left(\frac{\partial^2\bar{u}}{\partial\bar{r}^2}-\frac{\lambda_2\partial\bar{w}}{\lambda_1\partial\bar{r}}+\frac{\partial\bar{w}}{\partial\bar{r}}\frac{\partial^2\bar{w}}{\partial\bar{r}^2}\right)+\bar{D}_{11}\frac{\partial^2\bar{\phi}}{\partial\bar{r}^2}+\bar{B}_{12}\left(\frac{\partial\bar{u}}{\bar{r}\partial\bar{r}}-\frac{\bar{u}}{\bar{r}^2}-\frac{\lambda_2\partial\bar{w}}{\lambda_1\partial\bar{r}}\right)\right.\\&\left.+\bar{D}_{12}\left(\frac{\partial\bar{\phi}}{\bar{r}\partial\bar{r}}-\frac{\bar{\phi}}{\bar{r}^2}\right)\right]-\frac{1}{\lambda_1^2}\left[\int_{-1/2}^{1/2}\left(\bar{C}_{11}+\bar{C}_{12}\right)\alpha T\mathrm{d}\bar{z}-\int_{-1/2}^{1/2}\left(\bar{C}_{21}+\bar{C}_{22}\right)\alpha T\mathrm{d}\bar{z}\right]\\&-\frac{\bar{r}\bar{G}}{\lambda_1^2}\left(\bar{\phi}+\frac{\partial\bar{w}}{\partial\bar{r}}\right)=\bar{I}_1\bar{r}\frac{\partial^2\bar{u}}{\partial\tau^2}+\bar{I}_2\bar{r}\frac{\partial^2\bar{\phi}}{\partial\tau^2}\end{aligned} \tag{17}$$

The dimensionless initial conditions ($\tau=0$) are

$$\bar{w}=0,\quad \frac{\partial\bar{w}}{\partial\tau}=0,\quad \bar{u}=0,\quad \frac{\partial\bar{u}}{\partial\tau}=0,\quad \bar{\phi}=0,\quad \frac{\partial\bar{\phi}}{\partial\tau}=0 \tag{18}$$

Four types of boundary conditions for the shallow spherical shell are expressed as

(1) Clamped shallow spherical shell with immovable in-plane boundary conditions at $\bar{r} = 1$:

$$\bar{r} = 0: \quad \bar{u} = 0, \quad \frac{\partial \bar{w}}{\partial \bar{r}} = 0, \quad \bar{\phi} = 0 \tag{19}$$

$$\bar{r} = 1: \quad \bar{u} = 0, \quad \bar{w} = 0, \quad \bar{\phi} = 0 \tag{20}$$

(2) Clamped shallow spherical shell with movable in-plane boundary conditions at $\bar{r} = 1$:

$$\bar{r} = 0: \quad \bar{u} = 0, \quad \frac{\partial \bar{w}}{\partial \bar{r}} = 0, \quad \bar{\phi} = 0 \tag{21}$$

$$\bar{r} = 1: \quad N_\varphi = 0, \quad \bar{w} = 0, \quad \bar{\phi} = 0 \tag{22}$$

(3) Simply supported shallow spherical shell with immovable in-plane boundary conditions at $\bar{r} = 1$:

$$\bar{r} = 0: \quad \bar{u} = 0, \quad \frac{\partial \bar{w}}{\partial \bar{r}} = 0, \quad \bar{\phi} = 0 \tag{23}$$

$$\bar{r} = 1: \quad \bar{u} = 0, \quad \bar{w} = 0, \quad M_\varphi = 0 \tag{24}$$

(4) Simply supported shallow spherical shell with movable in-plane boundary conditions at $\bar{r} = 1$:

$$\bar{r} = 0: \quad \bar{u} = 0, \quad \frac{\partial \bar{w}}{\partial \bar{r}} = 0, \quad \bar{\phi} = 0 \tag{25}$$

$$\bar{r} = 1: \quad N_\varphi = 0, \quad \bar{w} = 0, \quad M_\varphi = 0 \tag{26}$$

III. METHOD OF SOLUTION

The unsteady heat transfer equation and nonlinear governing equations of motion for the FG shallow spherical shell are complicated, so approximate methods are employed to numerically solve the complicated problems.

The finite difference method is used here to discretize the unsteady heat transfer equation. The thickness is subdivided into L sections of equal thickness $\Delta z = h/L$, and the time increment is $\Delta\tau$. According to Eq.(5), at each time incremental interval, the temperature at any nodal location l ($0 \leq l \leq L$) can be derived as

$$\begin{aligned} T(l, \tau + \Delta\tau) = {} & T(l, \tau) + \frac{\Delta\tau}{\rho(l,\tau)\, c(l,\tau)} \left\{ \frac{1}{2\Delta z} \frac{\partial k(l,\tau)}{\partial z} \left[T(l+1,\tau) - T(l-1,\tau) \right] \right. \\ & \left. + \frac{k(l,\tau)}{(\Delta z)^2} \left[T(l+1,\tau) + T(l-1,\tau) - 2T(l,\tau) \right] \right\} \end{aligned} \tag{27}$$

The dimensionless unknown displacement functions $\bar{u}$, $\bar{w}$ and $\bar{\phi}$ are divided between space and time, respectively. A set of finite degree polynomials in $\bar{r}$ are used to discretize the displacement functions in the space domain, that is

$$\bar{u}(\bar{r}) = \sum_{m=1}^{M+2} \bar{r}^{m-1} a_m, \quad \bar{w}(\bar{r}) = \sum_{p=1}^{M+2} \bar{r}^{p-1} b_p, \quad \bar{\phi}(\bar{r}) = \sum_{s=1}^{M+2} \bar{r}^{s-1} c_s \tag{28}$$

where M is the number of the discrete points $\bar{r}_i$ which, in the internal [0, 1], are taken at the zeros of a Chebyshev polynomial given by

$$\bar{r}_i = \frac{1}{2} \left\{ 1 + \cos \left[\frac{(2i-1)\pi}{2M} \right] \right\} \quad (i = 1, 2, ..., M) \tag{29}$$

The inertia terms are discretized using the Newmark-beta method, for instance, the transverse inertia term can be expressed as

$$\begin{aligned} \left(\frac{\partial^2 \bar{w}}{\partial \tau^2} \right)_J &= \frac{4(\bar{w}_J - \bar{w}_{J-1})}{(\Delta\tau)^2} - \frac{4}{\Delta\tau} \left(\frac{\partial \bar{w}}{\partial \tau} \right)_{J-1} - \left(\frac{\partial^2 \bar{w}}{\partial \tau^2} \right)_{J-1} \\ \left(\frac{\partial \bar{w}}{\partial \tau} \right)_J &= \left(\frac{\partial \bar{w}}{\partial \tau} \right)_{J-1} + \frac{1}{2} \left[\left(\frac{\partial^2 \bar{w}}{\partial \tau^2} \right)_{J-1} + \left(\frac{\partial^2 \bar{w}}{\partial \tau^2} \right)_J \right] (\Delta\tau) \end{aligned} \tag{30}$$

The whole equations are solved iteratively. In each iterative step J, the nonlinear terms in Eqs.(15), (16), (17) and boundary conditions are linearized and transformed into

$$(x \cdot y)_J = (x)_J \cdot (y)_{J_P} \tag{31}$$

where $(y)_{J_P}$ is the average value of those obtained in the previous two iterations. For the initial iterative step, it can be determined by using quadratic extrapolation, that is

$$(y)_{J_P} = A\,(y)_{J-1} + B\,(y)_{J-2} + C\,(y)_{J-3} \tag{32}$$

For different iterative steps, the coefficients A, B and C are

$$\begin{aligned} &J=1: \quad A=1, \quad B=0, \quad C=0 \\ &J=2: \quad A=2, \quad B=-1, \quad C=0 \\ &J=3: \quad A=3, \quad B=-3, \quad C=1 \end{aligned} \tag{33}$$

Substituting Eqs.(27), (29), (30) and (31) into the nonlinear governing equations of motion (15), (16), (17) and boundary conditions, and using the initial conditions (18), we can get $3M+6$ linear algebraic equations. For every iterative step, the iteration lasts until the difference between the present value and the former is smaller than 0.01%. After the convergent values of a_m, b_p and c_s are obtained at the J th step, the displacements can be determined, the current iteration step stops and the next iteration step begins.

IV. NUMERICAL EXAMPLES

In order to verify the present analysis, firstly, the central temperature distribution through the thickness of FG shell is compared with the results obtained by Qian et al.[17] in Fig.2. It is observed that the two results are in good agreement at different time. Secondly, the radius of curvature of a FG shallow spherical shell is taken as infinite, and the volume fraction index n is taken as zero. Then the FG shallow spherical shell degenerates to a homogeneous and isotropic circular plate. Considering the dynamic response of a circular plate with clamped boundary conditions subjected to a uniform load, Fig.3 presents the comparisons of the central deflection w_0 obtained by current analysis with reference to Ref.[22]. From the figure, it can be seen that the two results agree well with each other except for a slight difference, showing that the present analysis yields acceptable results.

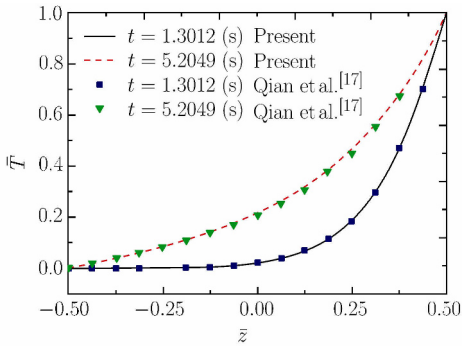

Fig. 2. Comparison of central temperature through the thickness of the structure at different time.

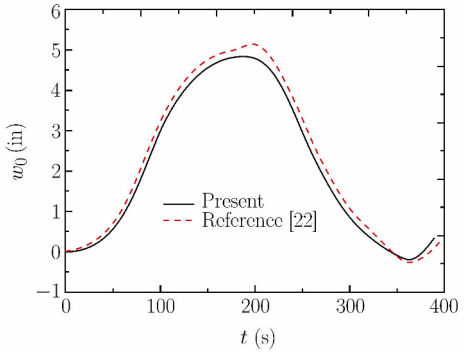

Fig. 3. Comparison of central deflection versus time for a circular plate under a uniform load.

In the following numerical calculations, a FG shallow spherical shell clamped with in-plane immovable composed of aluminium and alumina is considered. The material properties of the aluminium and alumina are listed in Table 1. The shear correction factor is 5/6. And the curvature radius of the middle curved surface, the thickness of the shell and the radius of the base circle for the shell are taken as $R=4$, $h=0.06$, and $a=0.3$, respectively. The prescribed temperature on the bottom surface of the shell is

maintained at the stress free temperature, while the prescribed temperature on the top surface of the shell increases exponentially from the stress-free temperature given by

$$T_t = T_0(1 - \mathrm{e}^{-\gamma t}) \tag{34}$$

where T_0 denotes the characteristic temperature, and γ denotes the rate of temperature change on the top surface and is defined as a temperature coefficient. The dimensionless temperature can be expressed as $\bar{T} = T/T_0$. All the results below are presented with respect to the dimensional parameters.

Table 1. **Materials properties of aluminium and alumina in FG shallow spherical shell**

Materials	Poisson's ratio ν	Young's modulus E (GPa)	Mass density ρ (kg/m^3)	Thermal conductivity k (W/mK)	Specific heat c (J/kgK)	Coefficient of thermal expansion $\alpha(/K)$
Aluminium	0.3	70	2700	204	880	0.000023
Alumina	0.3	380	3800	10.4	205	0.0000074

The effects of geometric nonlinearity on the nonlinear dynamic response of FG shallow spherical shells subjected to a thermal or mechanical load are studied. Figure 4 shows the comparison of dynamic response of FG shallow spherical shells with different volume fraction index subjected to thermal load obtained by the nonlinear analysis to linear analysis. The characteristic temperature and temperature coefficient are $T_0 = 1500$ K and $\gamma = 10$, respectively. Figure 5 shows the comparison of dynamic response of FG shallow spherical shells with different volume fraction indices subjected to a mechanical load obtained by nonlinear analysis and linear analysis. The dimensionless uniform load $\bar{q} = 1$. From Figs.4 and 5, one can see the linear analysis underestimates the deflection of shallow spherical shells subjected to thermal loads or mechanical loads. And from the available literature [23, 24], one can find that the linear analysis also underestimates the deflection by the static and dynamic analysis of spherical shell subjected to mechanical loads. This result of the spherical shell is different from that of the plate whose deflection the linear analysis always overestimates[23, 24].

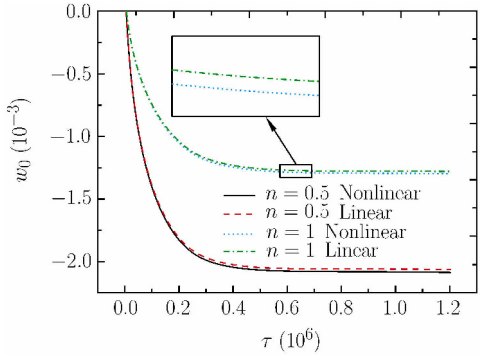

Fig. 4. Comparison of central deflection versus time for FG shallow spherical shells subjected to thermal load obtained by the nonlinear analysis to linear analysis.

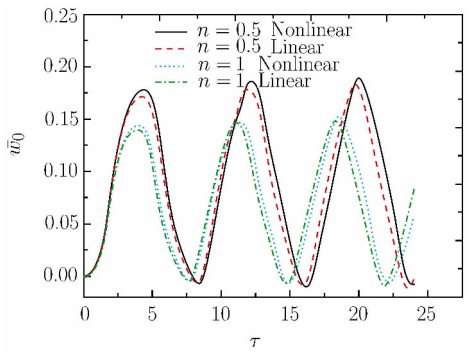

Fig. 5. Comparison of central deflection versus time for FG shallow spherical shells subjected to uniform load obtained by the nonlinear analysis to linear analysis.

For the FG shallow spherical shell with the volume fraction index $n = 1$, Fig.6(a) shows the time histories of the temperature on the middle plane for different temperature coefficients $\gamma = 0.1$, 0.5, 10 and ∞. T_0 is taken as 200 K. It can be seen that the temperature rises from 0 to a steady-state value as do different γ s. And the temperature reaches the steady state faster with an increase in γ. Note that for $\gamma = 10$ and ∞, the temperature changes have the same trend. Figure 6(b) illustrates the temperature distribution through thickness at time $\tau = 0.02 \times 10^6$, 0.08×10^6, 0.24×10^6, 0.6×10^6 and 1.2×10^6 for $\gamma = 10$. The temperature distribution through thickness remains the same when the time is 0.6×10^6 and 1.2×10^6, showing that the temperature has reached the steady state at $\tau = 0.6 \times 10^6$.

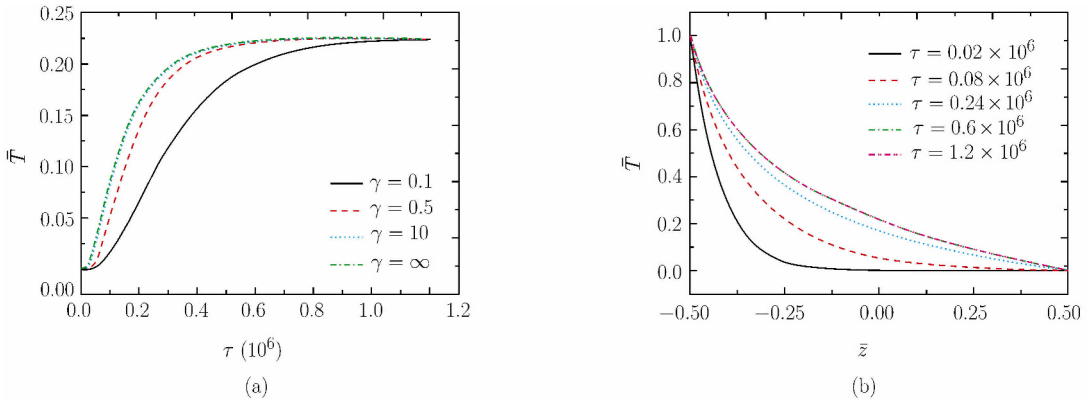

Fig. 6. (a) Temperature on the middle plane versus time for FG shallow spherical shell with different temperature coefficients $\gamma = 0.1$, 0.5, 10 and ∞; (b) Temperature through the thickness of the shell with at various time $\tau = 0.02 \times 10^6$, $\tau = 0.08 \times 10^6$, $\tau = 0.24 \times 10^6$, $\tau = 0.6 \times 10^6$ and $\tau = 1.2 \times 10^6$.

The time histories of the central deflection $\bar{w}_0$, the axial stress $\bar{\sigma}_r$, the circumferential stress $\bar{\sigma}_\theta$ and the transverse shear stress $\bar{\sigma}_{rz}$ in the center of the middle plane for FG shallow spherical shell with the volume fraction index $n = 1$ for different temperature coefficients $\gamma = 0.1$, 0.5, 10 and ∞ are exhibited in Fig.7. It is clear that the central deflection and stresses are virtually the same for $\gamma = 10$ and ∞. Moreover, it can be seen from the figures that the magnitude of the central deflection, the axial stress, the circumferential stress and the transverse shear stress rises with time to the steady-state values, which takes a shorter time with an increase of the temperature coefficient γ.

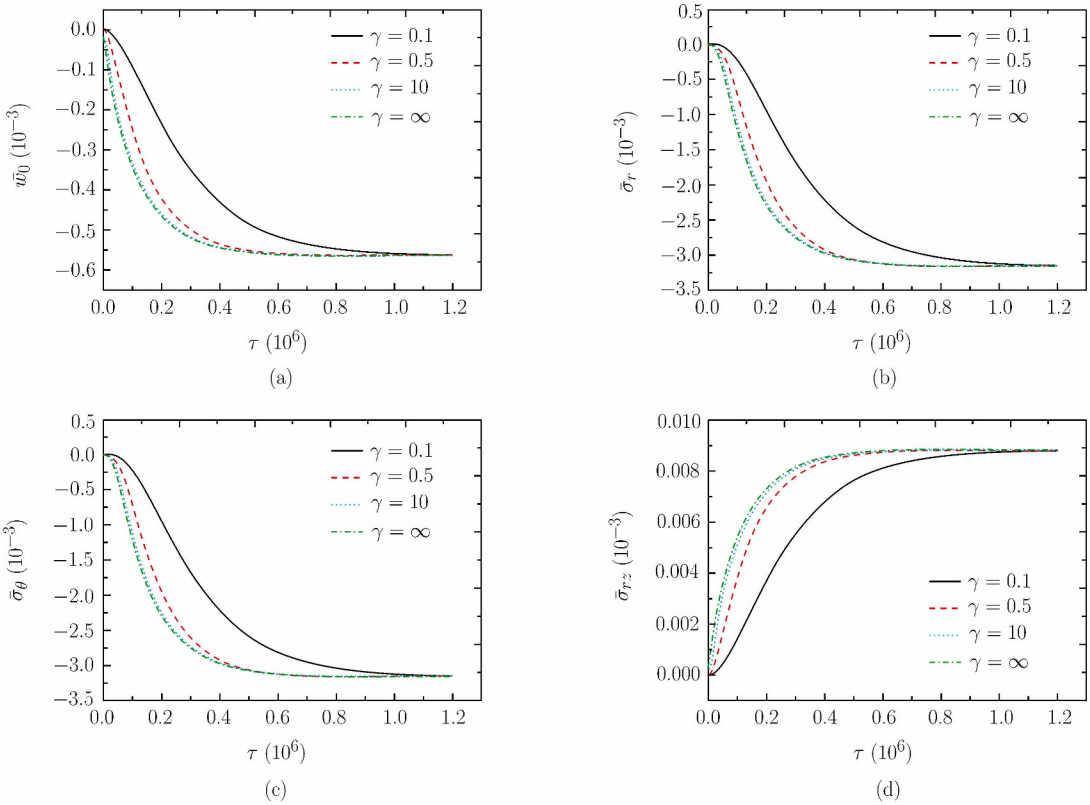

Fig. 7. (a) Central deflection, (b) axial stress, (c) circumferential stress and (d) transverse shear stress versus time for FG shallow spherical shell with the volume fraction index $n = 1$ for different temperature coefficients $\gamma = 0.1$, 0.5, 10 and ∞.

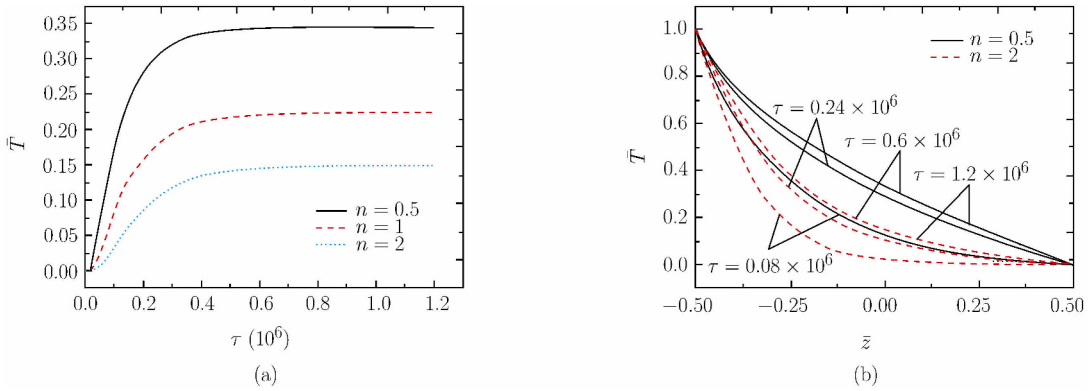

Fig. 8. (a) Temperature on the middle plane versus time for FG shallow spherical shell with different volume fraction indices $n = 0.5$, 1, and 2, (b) temperature through the thickness of the shell with $n = 0.5$, 1, and 2 for $\gamma = 10$ at various time $\tau = 0.02 \times 10^6$, 0.08×10^6, 0.6×10^6 and $\tau = 1.2 \times 10^6$ under the unsteady temperature field condition with the temperature coefficient $\gamma = 10$.

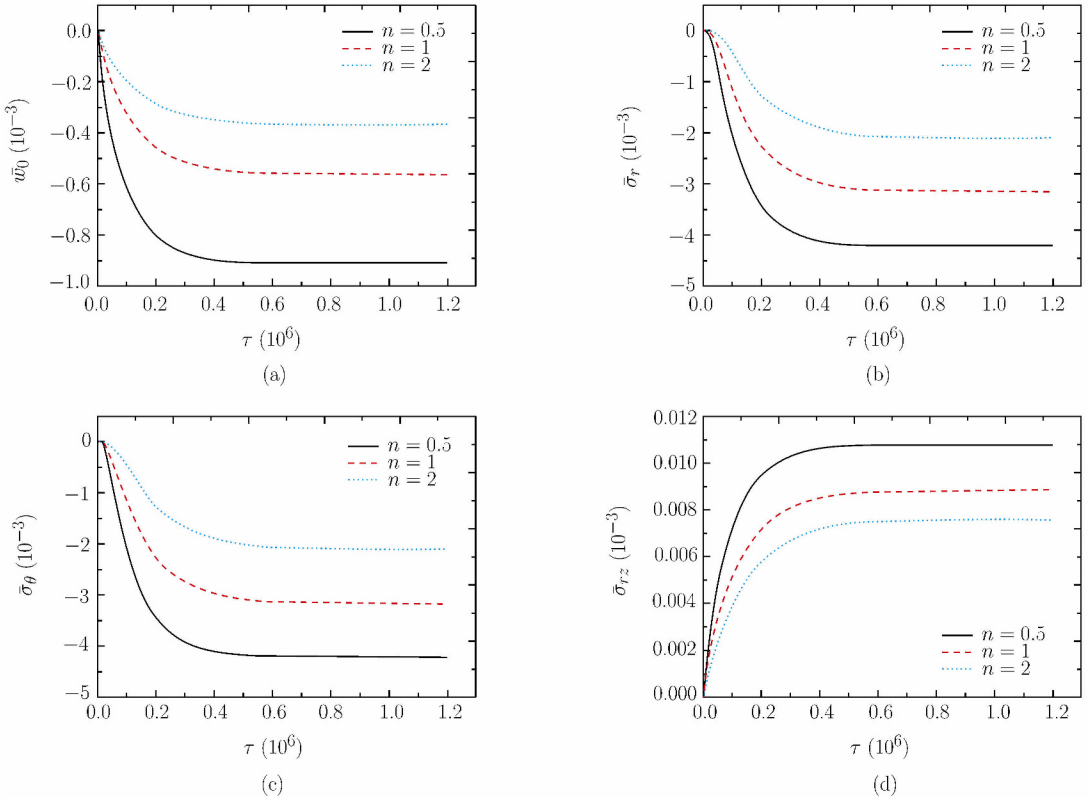

Fig. 9. (a) Central deflection, (b) axial stress, (c) circumferential stress and (d) transverse shear stress versus time for FG shallow spherical shell with different volume fraction index $n = 0.5$, 1, and 2 under the unsteady temperature field condition with the temperature coefficient $\gamma = 10$.

In the unsteady temperature field with the temperature coefficient $\gamma = 10$ and T_0 taken as 200 K, the influence of the volume fraction index n on the temperature in the center of the middle plane and through the thickness for the FG shallow spherical shell are shown in Fig.8(a) and Fig.8(b), respectively. The temperature decreases and reaches a steady-state value faster with an increase in the volume fraction index. The reason is that the shell is richer in ceramic with the volume fraction index increase, which leads to the thermal load lower in the shell. Therefore, as shown in Fig.9, the magnitude of the central deflection $\bar{w}_0$, the axial stress $\bar{\sigma}_r$, the circumferential stress $\bar{\sigma}_\theta$ and the transverse shear stress $\bar{\sigma}_{rz}$

decreases as the volume fraction index is increased. From Fig.9(b) and (c), note that the axial stress and the circumferential stress are almost equal and have a similar variation tendency with time. And it can be seen from Fig.9(a) and (d) that the transverse shear stress has a similar evolution with the central deflection during the variation of volume fraction index, which shows that the transverse shear stress plays a dominant role in the nonlinear dynamic response of the FG shell in the unsteady temperature field.

For a study of nonlinear dynamic response of the FG shallow spherical shell subjected to uniform load under an unsteady temperature field, the uniform mechanical load applied on the top surface of the shell is taken as $\bar{q} = q_0 \sin(0.02\pi\tau)$, where q_0 is the dimensional load amplitude. And the characteristic temperature, temperature coefficient and the volume fraction index are $T_0 = 200$ K, $\gamma = 10$ and $n = 1$, respectively. Figure 10 shows the time histories of the central deflection $\bar{w}_0$, the axial stress $\bar{\sigma}_r$, the circumferential stress $\bar{\sigma}_\theta$ and the transverse shear stress $\bar{\sigma}_{rz}$ in the center of the middle plane for $q_0 = 0.05$, 0.1 and 0.2. Obviously, as shown in Fig.10(a), the central deflection increases with an increase in mechanical load, but the response cycle is the same. And the transverse shear stress has a similar tendency as shown in Fig.10(d). It can be seen from Fig.10(b) and (c) that the axial stress and the circumferential stress increase at the time interval $[0,\ 0.4 \times 10^6]$ before the temperature reaches the steady state. After that, the axial stress and the circumferential stress vary with time periodically. But the magnitude of the axial stress and the circumferential stress have risen slightly compared with the axial stress and the circumferential stress produced by the temperature field shown in Fig.7(b) and (c), which indicates the thermal load plays a domination role in the axial stress and the circumferential stress.

The effects of the volume fraction index on the central deflection $\bar{w}_0$, the axial stress $\bar{\sigma}_r$, the circumferential stress $\bar{\sigma}_\theta$ and the transverse shear stress $\bar{\sigma}_{rz}$ in the center of the middle plane for the FG shallow spherical shell are shown in Fig.11. The characteristic temperature, temperature coefficient and

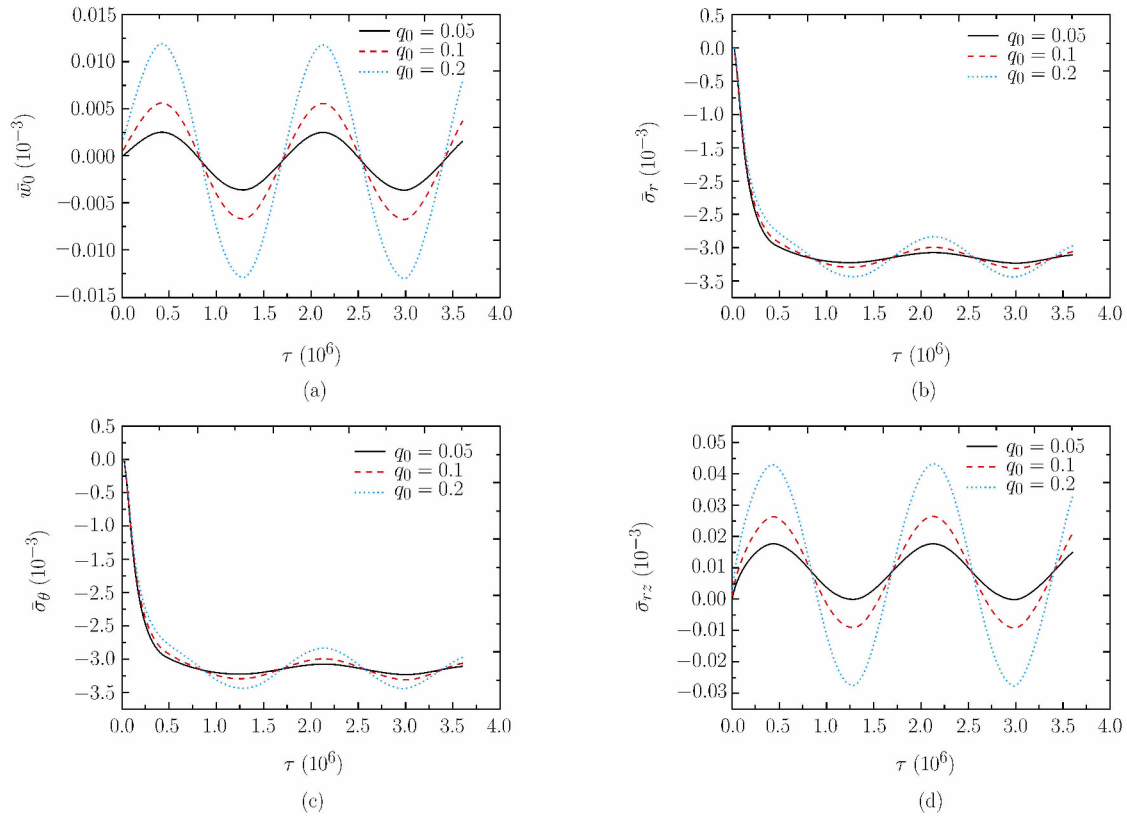

Fig. 10. (a) Central deflection, (b) axial stress, (c) circumferential stress and (d) transverse shear stress versus time for FG shallow spherical shell with volume fraction index $n = 1$ subjected to different mechanical load with dimensional load amplitude $q_0 = 0.05$, 0.1, and 0.2 under unsteady temperature field condition with the temperature coefficient $\gamma = 10$.

the dimensional load amplitude are $T_0 = 200$ K, $\gamma = 10$ and $q_0 = 0.1$, respectively. For a variety of volume fraction indices $n = 0.5$, 1 and 2, the response cycles for the central deflection and the stresses are the same. The magnitude of maximum central deflection decreases sharply with an increase in the volume fraction index shown in Fig.11(a). The reason is that the thermal load decreases whilst the stiffness of the shell increases as the volume fraction index is increased. And the upward central deflection is larger and lasts longer than the downward central deflection. Figure 11(b) and (c) illustrate the magnitude of axial stress and circumferential stress also declines with the volume fraction index increasing. However, as shown in Fig.11(d) the magnitude of negative transverse shear stress increases while positive transverse shear stress nearly remains stable with the volume fraction index increasing throughout the procedure.

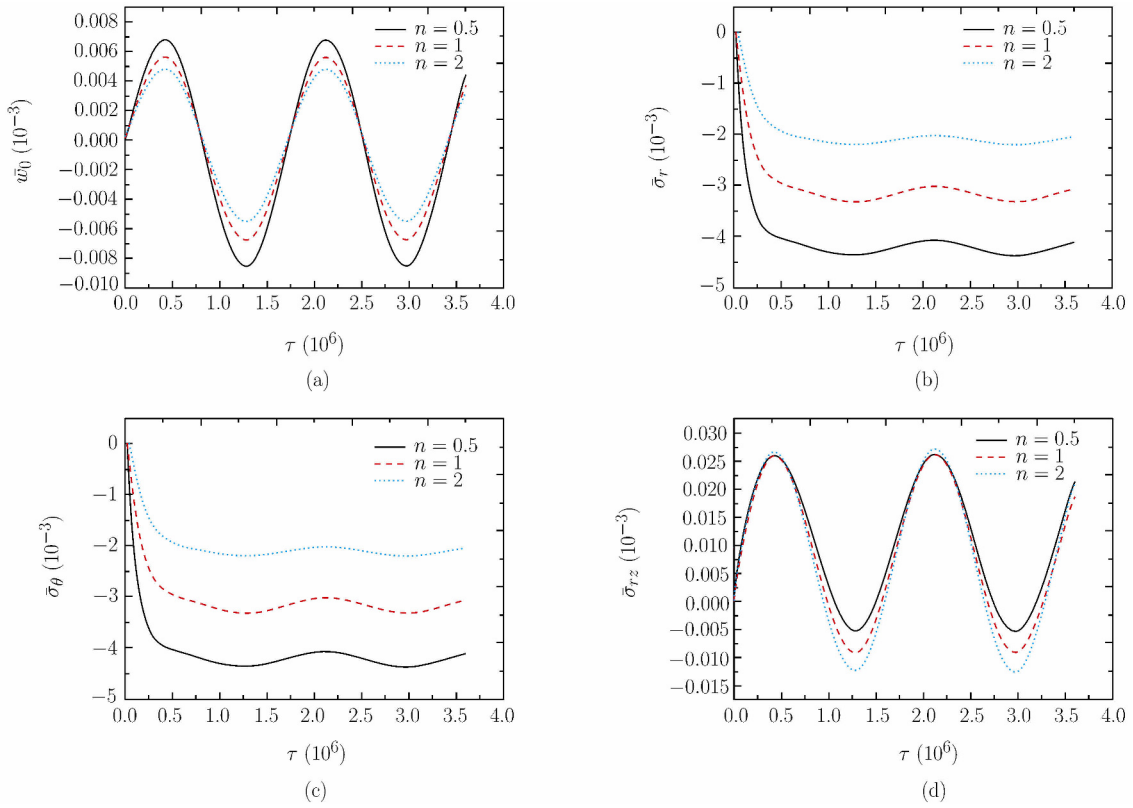

Fig. 11. (a) Central deflection, (b) axial stress, (c) circumferential stress and (d) transverse shear stress versus time for FG shallow spherical shell with different volume fraction indicees $n = 0.5$, 1, 2. The shell is subjected to thermomechanical load with the dimensional load amplitude $q_0 = 0.1$ and the temperature coefficient $\gamma = 10$.

V. CONCLUSIONS

In this paper, nonlinear governing equations of motion including transverse shear deformation and rotary inertia are presented for FG shallow shells subjected to time- dependent thermomechanical loads. The nonlinear governing equations of motion are numerically solved along with the unsteady heat transfer equation. And the transient deflection and stresses of the FG shallow spherical shell are analyzed. The main conclusions can be drawn as follows: The geometric nonlinearity of FG shallow spherical shells contributes to overestimating the deflection in contrast to the linear analysis. When the shell is assigned a certain temperature on the top surface and one on the bottom surface is maintained at the stress free temperature, the temperature on an arbitrary point in the shell increases from 0 to a steady-state value. And the increasedvolume fraction index of the shell contributes to reducing the temperature in the shell, which makes the shell more resistant to the external temperature. The upward

central deflection of FG shallow spherical shell under the thermomechanical load is greater and lasts longer than the downward central deflection. And the increase of the volume fraction index for the FG shallow spherical shell is able to effectively decrease the stresses whilst the central deflection markedly declines.

References

[1] Koizumi,M., FGM activities in Japan. *Composites Part B: Engineering*, 1997, 28(1): 1-4.

[2] Shen,H.S., Nonlinear bending response of functionally graded plates subjected to transverse loads and in thermal environments. *International Journal of Mechanical Sciences*, 2002, 44(3): 561-584.

[3] Pelletier,J.L. and Vel,S.S., An exact solution for the steady-state thermoelastic response of functionally graded orthotropic cylindrical shells. *International Journal of solids and structures*, 2006, 43(5): 1131-1158.

[4] Tarn,J.Q., Exact solutions for functionally graded anisotropic cylinders subjected to thermal and mechanical loads. *International Journal of Solids and Structures*, 2001, 38(46): 8189-8206.

[5] Woo,J., Meguid,S.A. and Stranart,J.C. et al., Thermomechanical postbuckling analysis of moderately thick functionally graded plates and shallow shells. *International Journal of Mechanical Sciences*, 2005, 47(8): 1147-1171.

[6] Ma,L.S. and Wang,T.J., Nonlinear bending and post-buckling of a functionally graded circular plate under mechanical and thermal loadings. *International Journal of Solids and Structures*, 2003, 40(13): 3311-3330.

[7] Alijani,F., Amabili,M. and Bakhtiari-Nejad,F., Thermal effects on nonlinear vibrations of functionally graded doubly curved shells using higher order shear deformation theory. *Composite Structures*, 2011, 93(10): 2541-2553.

[8] Shahsiah,R., Eslami,M.R. and Naj,R., Thermal instability of functionally graded shallow spherical shell. *Journal of Thermal Stresses*, 2006, 29(8): 771-790.

[9] Praveen,G.N. and Reddy,J.N., Nonlinear transient thermoelastic analysis of functionally graded ceramic-metal plates. *International Journal of Solids and Structures*, 1998, 35(33): 4457-4476.

[10] Wang,B.L., Mai,Y.W. and Zhang,X.H., Thermal shock resistance of functionally graded materials. *Acta materialia*, 2004, 52(17): 4961-4972.

[11] Goupee,A.J. and Vel,S.S., Transient multiscale thermoelastic analysis of functionally graded materials. *Composite Structures*, 2010, 92(6): 1372-1390.

[12] Kim,K.S. and Noda,N., A Green's function approach to the deflection of a FGM plate under transient thermal loading. *Archive of Applied Mechanics*, 2002, 72(2-3): 127-137.

[13] Tanigawa,Y., Akai,T. and Kawamura,R. et al., Transient heat conduction and thermal stress problems of a nonhomogeneous plate with temperature-dependent material properties. *Journal of Thermal Stresses*, 1996, 19(1): 77-102.

[14] Jin,Z.H. and Paulino,G.H., Transient thermal stress analysis of an edge crack in a functionally graded material. *International Journal of Fracture*, 2001, 107(1): 73-98.

[15] Asgari,M. and Akhlaghi,M., Transient thermal stresses in two-dimensional functionally graded thick hollow cylinder with finite length. *Archive of Applied Mechanics*, 2010, 80(4): 353-376.

[16] Vel,S.S. and Batra,R.C., Three-dimensional analysis of transient thermal stresses in functionally graded plates. *International Journal of Solids and Structures*, 2003, 40(25): 7181-7196.

[17] Qian,L.F. and Batra,R.C., Three-dimensional transient heat conduction in a functionally graded thick plate with a higher-order plate theory and a meshless local Petrov-Galerkin method. *Computational Mechanics*, 2005, 35(3): 214-226.

[18] Nemat-Alla,M., Ahmed,K.I.E. and Hassab-Allah,I., Elastic-plastic analysis of two-dimensional functionally graded materials under thermal loading. *International Journal of solids and Structures*, 2009, 46(14): 2774-2786.

[19] Geankoplis,C., Transport Processes and Separation Process Principles (includes unit operations). Prentice Hall Press, 2003.

[20] Reddy,J.N., Wang,C.M. and Kitipornchai,S., Axisymmetric bending of functionally graded circular and annular plates. *European Journal of Mechanics-A/Solids*, 1999, 18(2): 185-199.

[21] Fu,Y.M., Nonlinear Analyses of Laminated Plates and Shells with Damage. WIT Press, 2013.

[22] Hinton,E., The dynamic transient analysis of axisymmetric circular plates by the finite element method. *Journal of Sound and Vibration*, 1976, 46(4): 465-472.

[23] Bathe,K. and Bolourchi,S., A geometric and material nonlinear plate and shell element. *Computers & structures*, 1980, 11(1): 23-48.

[24] Reddy,J.N. and Chandrashekhara,K., Geometrically non-linear transient analysis of laminated, doubly curved shells. *International Journal of Non-Linear Mechanics*, 1985, 20(2): 79-90.